Computational study of structural stability, elastic, electronic, magnetic and thermodynamic properties of the Rh$_2$-based full-Heusler compounds: Rh$_2$MnZ (Z = Sn, Pb, Tl) by FP-LAPW method

B. Benichou[a,*], H. Bouchenafa[b], Z. Nabi[c], and B. Bouabdallah[c]

[a]*Department of Electronics, Faculty of Technology,*
Hassiba Benbouali University of Chlef, Chlef 02000, Algeria.
**e-mail: boucif_benichou@yahoo.fr*
[b]*Department of Physics, Faculty of Exact Sciences and Informatics,*
Hassiba Benbouali University of Chlef, 02000 Chlef, Algeria.
[c]*Computational Materials Physics Laboratory (CMPL), Materials and Sustainable Development Department,*
Faculty of Exact Sciences, Djillali Liabès University of Sidi Bel Abbès, Sidi Bel Abbès 22000, Algeria.

The structural, elastic, electronic and thermodynamic properties as well as the magnetism of the ternary full-Heusler alloys Rh$_2$MnZ (X = Sn, Pb and Tl) have been investigated by using the full-potential linearized augmented plane wave (FP-LAPW) method based on density functional theory (DFT) within the generalized gradient approximation (GGA). The AlCu$_2$Mn-type structure is energetically more favorable than the CuHg$_2$Ti-type structure for all the compounds studied here and found to be are ferromagnetic. The electronic structures calculations are found to exhibit a metallic character for all the herein studied compounds Rh$_2$MnZ (X = Sn, Pb and Tl) alloys. The magnetic properties reveal that the Mn atom is responsible for large magnetic moment. Moreover, the mechanical behavior shows that all studied compounds are mechanically stable, ductile and anisotopic in nature. The elastic and thermodynamic properties for Rh$_2$MnTl compound have not yet been established. The obtained results for various properties of the series of Rh$_2$MnZ (X = Sn, Pb and Tl) are compared with those found experimentally and theoretically.

1. Introduction

Full-Heusler compounds have recently attracted a strong attention for their relatively high Curie temperature and large magnetic moment [1-9], and for their useful applications as ferromagnetic shape memory alloys [10–12], spintronic devices [13] and magnetic actuator [14]. Amongst the full-Heusler alloys, the Rh containing compounds, which have recently investigated by many theoretical and experimental researchers [15-28] to determine different properties, was firstly studied by Suits [29] to investigate the magnetic and structural properties for ferromagnetic compounds of the form Rh$_2$MnX where X is Al, Ga, In, Tl, Sn, Pb, and Sb. He found that the exchange is described in terms of competing ferromagnetic Mn-Rh-Mn interactions and antiferromagnetic Mn-Mn interactions.

Afterwards, the electronic structure and magnetic moment of three Rh-based Heusler alloys Rh$_2$MnX, with X = Ge, Sn and Pb have been calculated using the tight binding linear muffin-tin orbital (TB-LMTO) method by Pugacheva *et al.,* [30]. These authors have found that the total magnetic moment increases with increasing atomic number of X. Not later, Jezierski *et al.,* [31] presented the influence of local ordering on the electronic and magnetic properties of Heusler-type alloys Rh$_2$TMSn (TM = Mn, Fe, Co, Ni, Cu) and Rh$_2$MnX (X = Al, Ga, In, Ge, Sb, Pb). The band structure and magnetic moments are calculated by the ab-initio spin-polarized tight binding linear muffin-tin orbital method (TB-LMPTO).

In addition, using the full-potential screened Korringa-Kohn-Rostoker method, Galanakis *et al.,* [32] have studied the full-Heusler alloys based on Co, Fe, Rh, and Ru. They show that many of these compounds show a half-metallic behavior. Later on, Klaer *et al.,* [33] have measured the localized magnetic moments in the Heusler alloy Rh$_2$MnGe by using, the X-ray magnetic circular dichroism (XMCD) of core-level absorption (x-ray absorption spectroscopy, XAS) spectra in the soft x-ray region has been measured for the ferromagnetic Heusler alloy Rh$_2$MnGe at the Rh $M_{3,2}$ and Mn $L_{3,2}$ edges. They have found that the orbital moments of the Rh 4d and Mn 3d states are very small.

Recently, Sanvito *et al.,* [34] have investigated the physical properties of Rh$_2$MnTi, Rh$_2$MnZr, Rh$_2$MnHf, Rh$_2$MnSc and Rh$_2$MnZn by using density functional theory. These authors have found that most of the known magnetic HAs are metallic. Faleev *et al.,* [35] have studied the origin of the tetragonal ground state of Rh$_2$-based Heusler compounds for both the regular and inverse structures and various magnetic configurations using the VASP program with project or augmented wave (PAW) potentials and Perdew-Burke-Ernzerhof (PBE) generalized-gradient-approximation (GGA) DFT functional.

More recently, a numerical work on the electronic and magnetic structural parameters of Rh_2MnTi crystal was carried out within the density functional theory level as implemented in all electron full-potential linearized augmented plane wave (FP-LAPW) method by Benzoudji *et al.,* [36]. The authors show that the calculated density of states (DOS) and band structure for Rh_2MnTi show the absence of energy band gap in their minority-spin channel which moves away half-metallic character. Aguilera-Granja *et al.,* [37] have performed first-principle calculations of the structural, electronic and magnetic properties of Heusler X_2MnZ with X = Fe, Co, Ni, Cu, Ru, Rh, Pd, Ag, Pt, Au and Z = Al, Si, Ga, Ge, In and Sn, using density functional theory (DFT) calculations, as implemented in the SIESTA code.

Very latterly, the structural, electronic, elastic, magnetic, and thermodynamic properties of full-Heusler alloys Rh_2MnZ (Z = Zr, Hf)) using first-principles calculations were studied by Mentefa *et al.,* [38]. The electronic properties reveled the metallic nature of the Heusler Rh_2MnZ (Z = Zr, Hf) alloys. The elastic properties confirmed the elastic stability of the two alloys. They show high rigidity, anisotropic, and little deformation and behave in ductile way. The magnetic properties confirmed the ferromagnetic state of both compounds. In another theoretical study, Güler *et al.,* [39] have investigated the electronic, elastic, optical and magnetic properties of Rh_2MnX (X = Ti, Hf, Sc, Zr, Zn) Heusler alloys. Their study show that all investigated alloys are mechanically stable and ductile. Also, they have a typical metallic behavior and show strong ferromagnetic ordering following the magnetic moment rank of Ti > Zr > Hf > Sc > Zn.

The aim of the current work is to better visualize the behavior of the structural stabilities, mechanical, electronic, magnetic and thermodynamic properties of three full Heusler alloys Rh_2MnSn, Rh_2MnPb and Rh_2MnTl which is rarely found in the literature, in particular the thermodynamic and thermal properties which are not available in the literature, in order to provide a good baseline data to experimentalists and to enrich the existing theoretical calculations on these materials for future investigations. For this, we have employed the full-potential linearized augmented plane wave (FP-LAPW) method as implemented in the WIEN2k code, in the framework of the density functional theory (DFT) within the GGA approximation.

The manuscript is organized as follows. Section 2 deals with computational procedure. Section 3 presents the results of the reported calculations and discussion. Finally, a brief conclusion is given in the last section.

2. Theoretical calculation details

In this work, the first-principles calculations are performed within the full potential linearized augmented plane wave (FP-LAPW) method [40] as implemented in the WIEN2k package [41], in the framework of the density functional theory (DFT) [42, 43]. The exchange-correlation functional was calculated using the generalized gradient approximation (GGA) in the parameterization of Perdew-Burke-Ernzerhof (PBE) [44]. The plane wave parameter $R_{MT} \times K_{\max} = 7$ was used, where R_{MT} is the average radius of muffin-tin spheres and $K_{\max}$ is the largest K vector in the plane wave. To ensure the correctness of the calculations, we have taken $l_{\max}=10$ inside of the muffin tin spheres. The $G_{\max}$ parameter, which defined as the magnitude of largest vector in charge density Fourier expansion, was taken to be 12 a.u^{-1}. The separation energy between the core and the valence states was chosen as -7.0 Ry. The atomic sphere radii used are for Rh_2MnSn; $R_{MT}(Rh)= R_{MT}(Mn)= R_{MT}(Sn) = 2.41$, for Rh_2MnPb; $R_{MT}(Rh) = 2.39$, $R_{MT}(Mn) = 4.45$, $R_{MT}(Pb) = 2.5$ and for Rh_2MnTl, $R_{MT}(Rh) = 2.38$, $R_{MT}(Mn) = 2.44$, $R_{MT}(Tl) = 2.5$ a.u (atomic unit). The sampling of the Brillouin zone was done with a $12 \times 12 \times 12$ mesh, which gives convergence of 10^{-4} Ry in the total energy.

3. Crystal structure

Full-Heusler alloys possess an X_2YZ generic formula, where X and Y denote transition metals and Z is the main group element. The full Heusler compounds crystallize either in the
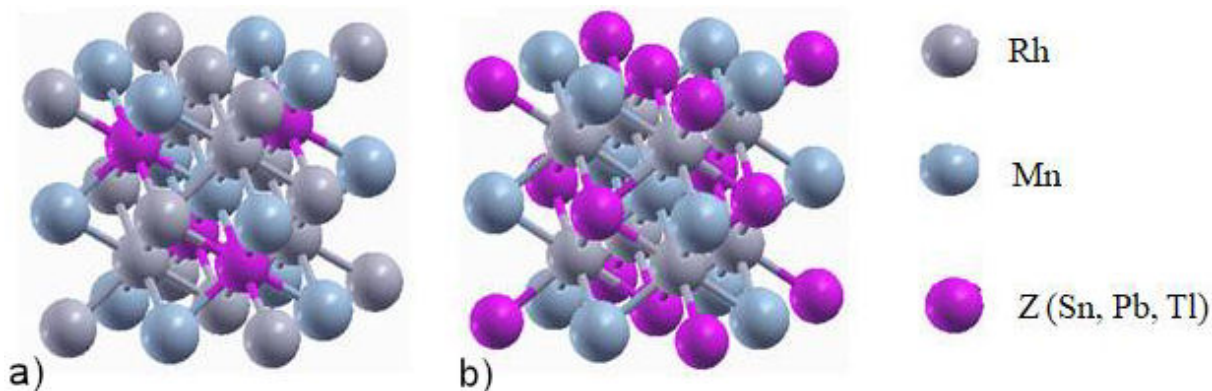

FIGURE 1. Crystal structure of Rh_2MnZ (Z = Sn, Pb,Tl) compounds. a) $CuHg_2Ti$ and b) $AlCu_2Mn$. These figures are plotted by using XCrySDen [45].
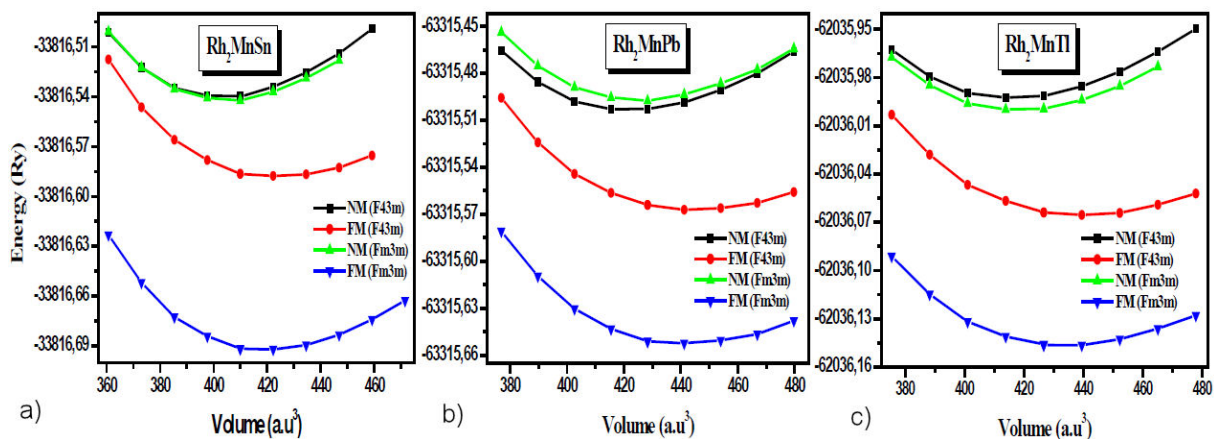
FIGURE 2. Variation of total energy as a function of lattice constant for both nonmagnetic (NM) and ferromagnetic (FM) states for $CuHg_2Ti$-type and $AlCu_2Mn$-type phases of a) Rh_2MnSn, b) Rh_2MnPb, and c) Rh_2MnTl alloys.

$L2_1$ cubic structure with $AlCu_2Mn$ as the prototype or in the inverse Heusler structure (Xa) with $CuHg_2Ti$ as prototype. In Fig. 1, we show the crystal structure of Rh_2MnZ alloys, where the present structures composed of four interpenetrating face-centered-cubic (fcc) sublattices. In $L2_1$ phase with the Fm-3m space group (no. 225), X atoms occupy A (0, 0, 0) and C (1/2, 1/2, 1/2) sites while the Y and Z atoms are located on B (1/4, 1/4, 1/4) and D (3/4, 3/4, 3/4) sites, respectively, in Wyckoff coordinates. In the $CuHg_2Ti$-type full Heusler alloy with the F43-m space group (no. 216), X atoms are located at the non-equivalent A (0, 0, 0) and B (1/4, 1/4, 1/4) sites, Y atom occupies C (1/2, 1/2, 1/2) site and Z atom occupies D (3/4, 3/4, 3/4) site.

4. Results and discussions

4.1. Structural properties

In the first step of the current study, we have performed calculations on the Rh_2MnZ (Z = Sn, Pb, Tl) ternary Heusler alloys, in both full (regular) Heusler ($AlCu_2Mn$-type ($L2_1$)) and inverse Heusler ($CuHg_2Ti$-type (Xa)) structural phases for non-magnetic (NM) and ferromagnetic (FM) configurations in order to determine the stable structure of the considered compounds. The calculated total energies variation within the GGA approximation versus the volume is plotted in Fig. 2. It is clearly seen from Fig. 2, that the ferromagnetic state is the most stable states as compared to the other states in the $AlCu_2Mn$-type structure for all the studied compounds due to its lowest total energy. This result confirms that $L2_1$-type structure agrees quite well with previous experimental works reported by Pillay *et al.,* [17], Dhar *et al.,* [18], and Jha *et al.,* [19], and theoretical results of Jezierski *et al.,* [31] and Sanvito *et al.,* [34] using first-principle calculation methods based on the DFT. The calculated total unit cell energy as a function of unit cell volume is fitted to Murnaghan's equation of state [46] to obtain ground state properties, such as the equilibrium lattice constants, the bulk modulus B and its pressure derivative B'.

The computed structural parameters for the ferromagnetic Rh_2MnZ (Z = Sn, Pb and Tl) compounds using the GGA are given in Table I. Our results for the lattice parameter are in reasonable agreement with previously obtained experimental data and theoretical calculations reported by other researchers for the present investigated compounds.

4.2. Elastic and mechanical properties

The computed three independent elastic constants C_{11}, C_{12}, and C_{44} of Rh_2MnZ (Z = Sn, Pb, Tl), from first-principle calculations, at an ambient pressure compared to other theoretical data are reported in Table II. The bulk modulus calculated from the theoretical values of the elastic constants $B = (1/3)/(C_{11} + 2C_{12})$ are also given in Table II. The traditional mechanical stability conditions in cubic crystals at equilibrium, which are known as the Born-Huang criteria [47], are defined in terms of elastic constants as follows: $C_{11} - C_{12} > 0$, $C_{44} > 0$, $C_{11} + 2C_{12} > 0$ and $C_{12} < B < C_{11}$ [48]. As can be seen, the elastic constants in Table II obey the above well known stability conditions, meaning that the cubic $L2_1$ phase is stable against elastic deformations at ambient conditions for the three compounds.

We note that the earlier ab-initio calculation on elastic properties for Rh_2MnSn and Rh_2MnPb compounds reported by Benkhelifa *et al.,* [24] and our results are in general in substantial agreement. Within best of knowledge, there is no report on the experimental and theoretical elastic constants and moduli available on Rh_2MnTl alloy in the literature for comparison. Therefore, our present results can be discussed as purely predictive.

Furthermore, we have derived and listed in Table III, other mechanical parameters namely shear modulus G, Young's modulus E, Poisson's ratio v, Zener anisotropy factor A and Kleinman parameter ξ for Rh_2MnZ (Z = Sn, Pb, Tl) within GGA, by using the Voigt-Reuss-Hill (VRH) averaging scheme [49–51]:

TABLE I. Optimized equilibrium lattice constant (a), bulk modulus (B), its pressure derivative (B') and total equilibrium energy E_0 for Rh$_2$MnZ (Z = Sn, Pb, Tl) Heusler compounds in non-magnetic (NM) and ferromagnetic (FM) states of both CuHg$_2$Ti and AlCu$_2$Mn-type structures.

Compound	structure	a(å)	B(GPa)	B'	E$_0$(Ry)
Rh$_2$MnSn	CuHg$_2$Ti (FM)	6.3086	151.8352	5.7888	-33816.588243
	CuHg$_2$Ti (NM)	6.2028	202.9067	5.7793	-33816.540315
	AlCu$_2$Mn (FM)	6.2921	177.4007	4.6825	-33816.692560
		6.25 [18]			
		6.232 [20]			
		6.23 [23]	195.55 [23]	5.55 [23]	
		6.233 [24]	191.132 [24]		
		6.252 [29]			
		6.239 [30]			
		6.35 [37]			
	AlCu$_2$Mn (NM)	6.2147	198.7040	4.6920	-33816.542129
Rh$_2$MnPb	CuHg$_2$Ti (FM)	6.4105	137.9806	5.8149	-63315.567127
	CuHg$_2$Ti (NM)	6.3001	181.3053	5.5093	-63315.503536
	AlCu$_2$Mn (FM)	6.3976	159.1320	5.1034	-63315.653000
		6.33 [18]			
		6.271 [20]			
		6.332 [24]	167.932 [24]		
		6.332 [29]			
		6.403 [30]			
		6.334 [31]			
	AlCu$_2$Mn (NM)	6.3172	178.2819	5.4172	-63315.497179
Rh$_2$MnTl	CuHg$_2$Ti (FM)	6.3875	141.0870	5.0567	-62036.065625
	CuHg$_2$Ti (NM)	6.2709	182.1366	5.1346	-62035.992866
	AlCu$_2$Mn (FM)	6.3576	150.6142	5.8206	-62036.146599
		6.324 [29]			
	AlCu$_2$Mn (NM)	6.2794	184.0574	5.2955	-62036.000368

$$G = \frac{G_V + G_R}{2}, \qquad (1)$$

$$G_V = \frac{C_{11} - C_{12} + 3C_{44}}{5}, \qquad (2)$$

$$G_R = \frac{5\left(C_{11} - C_{12}\right)C_{44}}{4C_{44} + 3\left(C_{11} - C_{12}\right)}, \qquad (3)$$

$$E = \frac{9BG}{3B + G}, \qquad (4)$$

$$v = \frac{3B - 2G}{2\left(3B + G\right)}, \qquad (5)$$

$$A = \frac{2C_{44}}{C_{11} - C_{12}}, \qquad (6)$$

$$\xi = \frac{C_{11} + 8C_{12}}{7C_{11} + 2C_{12}}. \qquad (7)$$

Where G_V is Voigt's shear modulus corresponding to the upper bound of G values and G_R is Reuss's shear modulus corresponding to the lower bound of G values.

The Cauchy pressure $C_P = C_{12} - C_{44}$ is an important parameter to identify the type of bonding [52]. If the Cauchy pressure is negative, the bonding is more directional and non-metallic in character, whereas positive value corresponds to a predominant metallic bonding. From Table III, all the studied compounds possess positive Cauchy pressure values, thus the predominant bonding for these compounds is metallic.

We note the higher bulk modulus and Young's modulus, which is an indication of a strong incompressibility for these compounds. Pugh [53] proposed an approximate criterion by the ratio of B/G to predict the brittle and ductile behavior of materials. Higher (lower) B/G ratio corresponds to ductile (brittle) behavior and the critical value that separates brittle

TABLE II. Calculated elastic constants (C_{ij}) and Bulk modulus (B) all expressed (in GPa) for Rh$_2$MnZ (Z = Sn, Pb, Tl) alloys in the AlCu$_2$Mn structure ferromagnetic (FM) ground state.

Compound	C_{11}	C_{12}	C_{44}	B
Rh$_2$MnSn	222.119	148.185	98.160	172.580
	234.43 [24]	170.46 [24]	114.73 [24]	191.78 [24]
Rh$_2$MnPb	177.977	126.598	96.263	143.710
	197.32 [24]	164.32 [24]	127.29 [24]	175.32 [24]
Rh$_2$MnTl	230.540	144.056	105.685	173.830

TABLE III. The calculated Cauchy pressure C_P, shear moduli G_V, G_R, G (in GPa) and B/G ratio, Young's modulus E (in GPa), Poisson's ratio v, shear anisotropic factor A and Kleinman parameter ξ for the Rh$_2$MnZ (Z = Sn, Pb, Tl) full-Heusler alloys.

Compound	C_P	G_V	G_R	G	B/G	E	v	A	ξ
Rh$_2$MnSn	50.02	73.68	59.05	66.36	2.60	176.48	0.32	2.65	0.76
		81.63 [24]	56.38 [24]	69.00 [24]	2.78 [24]	184.83 [24]	0.34 [24]	3.58 [24]	
Rh$_2$MnPb	30.33	68.03	45.86	56.94	2.52	150.91	0.32	3.74	0.79
		82.97 [24]	34.53 [24]	58.75 [24]	2.98 [24]	158.54 [24]	0.35 [24]	7.71 [24]	
Rh$_2$MnTl	38.37	80.70	66.99	73.84	2.35	149.05	0.31	2.44	0.72

and ductile materials is about 1.75. Therefore, our obtained results of B/G ratio suggest that all the herein studied compounds can be categorized as ductile materials.

The value of the Poisson's ratio is indicative of the degree of directionality of the covalent bonds. The typical value of the Poisson's ratio (v) for ionic materials is 0.25 [54]. The data in Table III indicate that Poisson's ratio vary from 0.313 to 0.329, which reveals that the interatomic forces are central forces [55]. It is clearly seen, from our calculated values of the Zener anisotropy factor A, which is a measure of the degree of elastic anisotropy of the crystal, that our Heusler alloys are elastically anisotropic.

Another important parameter is that of Young's modulus E which is the usual property used to characterize stiffness of a material. The greater the value of E, the stiffer is the material. From Table III, it is clearly seen that Rh$_2$MnSn is stiffer than Rh$_2$MnPb and Rh$_2$MnTl.

Once the values of young have been calculated, the Young's modulus E, bulk modulus B and the shear modulus G, we can easily compute the Debye temperature θ_D from the average sound velocity [56]:

$$\theta_D = \frac{h}{k} \left[\frac{3n}{4\pi} \left(\frac{N_A \rho}{M} \right) \right]^{1/3} \nu_m, \qquad (8)$$

where h is Plank's constant, k the Boltzmann constant, N_A the Avogadro number, ρ the density, M the molecular weight and n is the number of atoms in the molecule. To estimate the average sound velocity in the polycrystalline material, we have used the following equation [57]:

$$\nu_m = \left[\frac{1}{3} \left(\frac{2}{\nu_t^3} + \frac{1}{\nu_l^3} \right) \right]^{-1/3}, \qquad (9)$$

where ν_t and ν_l are the transverse and longitudinal elastic sound velocities obtained using the shear modulus G and the bulk modulus B from Navier's equation [58]:

$$\nu_t = \left(\frac{G}{\rho} \right)^{1/2}, \qquad (10)$$

$$\nu_l = \left(\frac{3B + 4G}{3\rho} \right)^{1/2}. \qquad (11)$$

The melting temperature is used in the heating system and can be theoretically estimated by the following equation [59]:

$$T_m = \left[553K + \left(\frac{5.91K}{GPa} \right) C_{11} \right] \pm 300K. \qquad (12)$$

In Table IV, we summarized the estimated elastic wave velocities, Debye temperature and predicted melting temperature for Rh$_2$MnZ (Z = Sn, Pb and Tl) Heusler alloys in their stable structure. It is clearly seen that Rh$_2$MnSn alloy exhibits the highest Debye temperature compared to those observed for Rh$_2$MnTl and Rh$_2$MnPb. It is also noted that the investigated compounds have higher values of melting temperature.

The obtained results for Rh$_2$MnSn and Rh$_2$MnPb alloys are in well agreement with earlier ab-initio calculation. As far as we know, the Rh$_2$MnTl compound is believed to be reported here for the first time.

4.3. Electronic properties

The total and partial density of states as a function of energy for the Rh$_2$MnZ (Z = Sn, Pb, Tl) Heusler alloys at its equilibrium lattice constant calculated using the GGA approximation are depicted in Fig. 3. As seen from Fig. 3, the intersection of both majority and minority spin band structures with
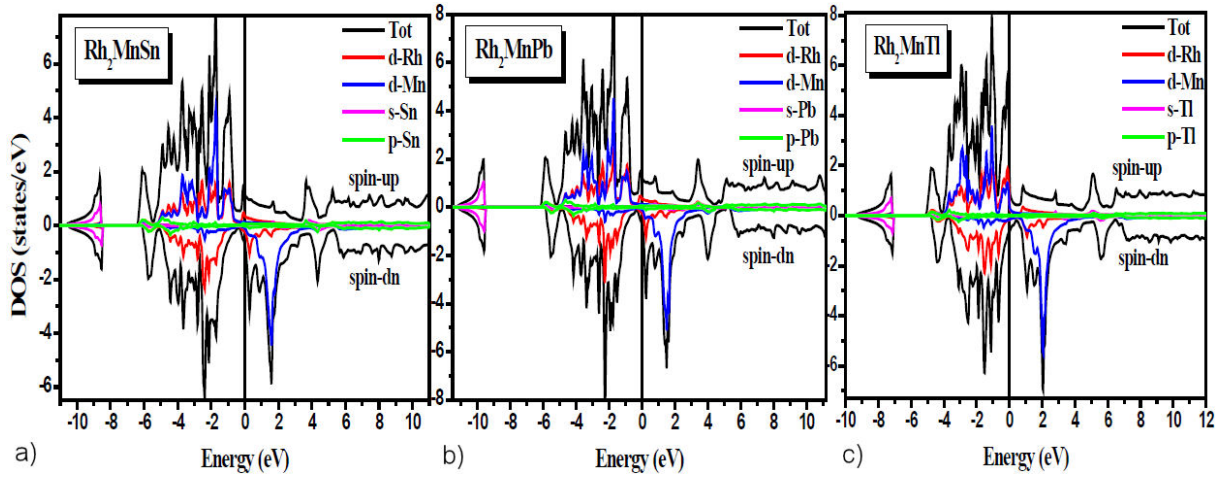
FIGURE 3. Total and partial density of states for a) Rh$_2$MnSn, b) Rh$_2$MnPb, and c) Rh$_2$MnTl Heusler alloys in their stable structure types.

TABLE IV. The calculated density ρ (in g·cm^{-3}), the transverse, longitudinal and average elastic wave velocities ν_t, ν_l and ν_m (in m·s^{-1}) and the Debye temperatures θ_D (in K) and melting temperatures T_m (in K) for Rh$_2$MnZ (Z = Sn, Pb and Tl) compounds.

Compound	ρ	ν_t	ν_l	ν_m	θ_D	$T_m \pm 300$
Rh$_2$MnSn	10.01	2552.66	4979.38	2861.04	338.68	1705.79
	10.408 [24]	2574.78 [24]	5221.64 [24]	2890.74 [24]	316.16 [24]	
					413 [15]	
Rh$_2$MnPb	11.87	2190.37	4301.16	2454.56	287.30	1476.70
	12.792 [24]	2143.06 [24]	4452.98 [24]	2409.24 [24]	263.21 [24]	
Rh$_2$MnTl	12.02	2478.67	4759.57	2775.75	327.55	1915.49

the Fermi level clearly reveals that all the herein compounds have metallic character. It is also clearly seen that the contributions to the resulting DOS are mainly formed by the Mn and Rh atoms around the Fermi level.

The analysis of the densities of electron states shows that there are two principal regions in the spin-up and spin-down states of DOS. The lower valence-bands below -8 eV for Rh$_2$MnSn (below -9 eV for Rh$_2$MnPb, below -7 eV for Rh$_2$MnTl) are merely due to the s-orbitals of the Sn, Pb and Tl atoms, whereas the next region localized between -6.5 and 5 eV for Rh$_2$MnSn (-6 to 5 eV for Rh$_2$MnPb and -5 to 5 eV for Rh$_2$MnTl) arise mostly from the 3d-states of the transition metals Rh/Mn. These obtained results for Rh$_2$MnZ are in fairly good accordance with other theoretical calculations [22–24, 30, 31, 37].

4.4. Magnetic properties

The calculated total and partial magnetic moments for the series of Rh$_2$MnZ (Z = Sn, Pb and Tl) in AlCu$_2$Mn-type structure are reported in Table V. As can be seen, the total magnetic moment composes the Rh atoms, the Mn atom, the Z atom, and the interstitial region. It can be clearly seen from Table V that the main magnetic moment resides at the Mn atom, because of the existence of a high exchange splitting between the majority and minority spin states of Mn atom. This behavior is also well known in most Heusler compounds

[60]. As listed in Table V, the local spin magnetic moment on the Rh and Mn atoms in these ferromagnetic compounds are positive, while Sn, Pb and Tl atoms have a negative and very small magnetic moment which can be neglectable. Furthermore, the values obtained of total and localized spin magnetic moments for the Heusler alloys under study agree quite well with the available experimental and theoretical data in the literature.

The Curie temperature (T_C) is calculated within the mean-field approximation (MFA) as follows [61]:

$$T_C = \frac{2}{3K_B}\Delta E. \qquad (13)$$

Where ΔE and K_B denote the total energy difference between antiferromagnetic and ferromagnetic configurations and the Boltzmann constant, respectively. The calculated values of the Curie temperature for Rh$_2$MnSn, Rh$_2$MnPb, and Rh$_2$MnTl are also listed in Table V.

4.5. Thermodynamic properties

In this section, we have used the quasi-harmonic Debye model as implemented in the Gibbs2 code [66, 67] to inspect the influence of high pressure from 0 to 30 GPa and high temperature from 0 to 1400 K at the behavior of Rh$_2$MnSn, Rh$_2$MnPb and Rh$_2$MnTl full-Heusler alloys being studied here.
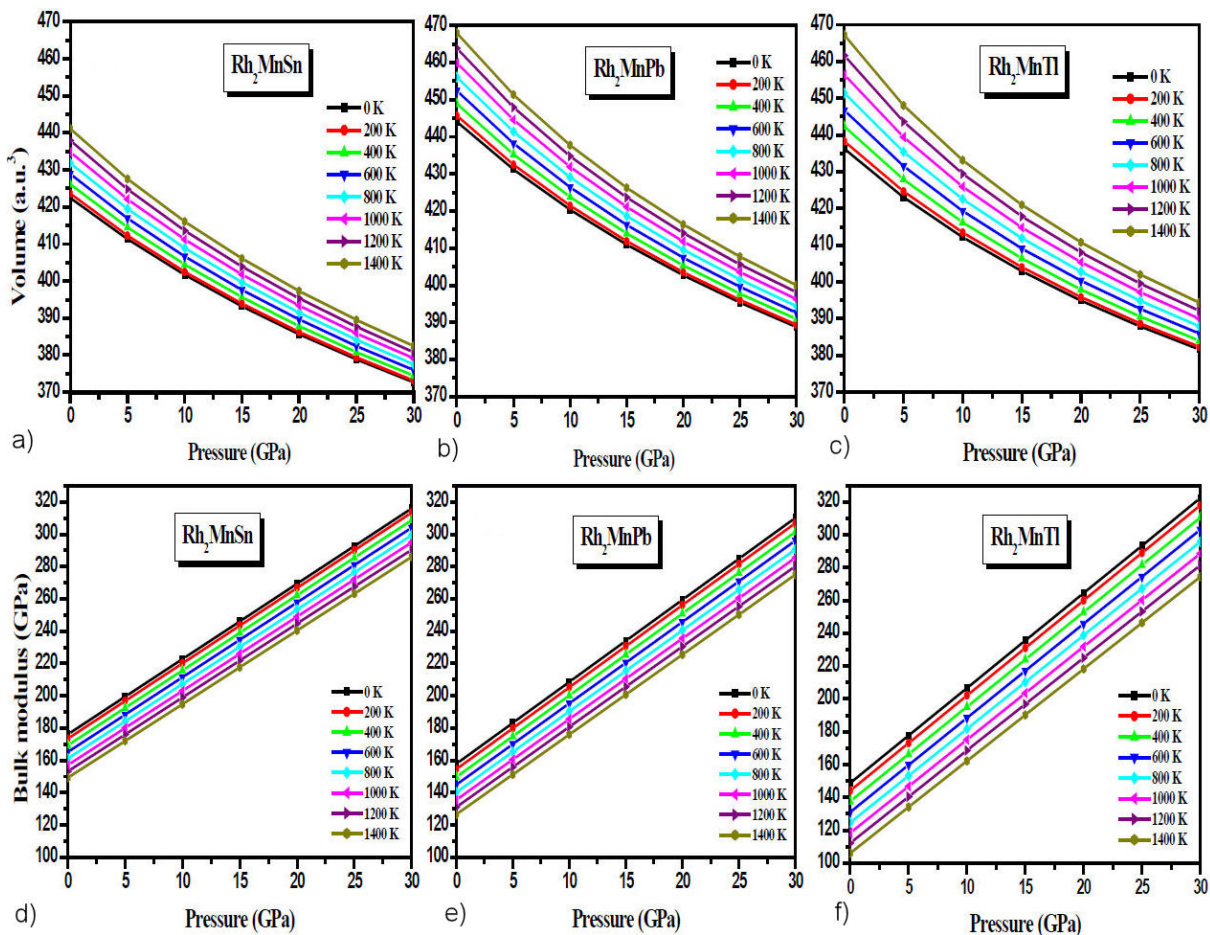
FIGURE 4. Variation of volume unit cell (V) for a) Rh_2MnSn, b) Rh_2MnPb, c) Rh_2MnTl, and bulk modulus (B) for d) Rh_2MnSn, e) Rh_2MnPb, and f) Rh_2MnTl as function of pressure for different temperatures.

TABLE V. Calculated local, interstitial and total spin magnetic moments (in μ_B), and Curie temperatures (in K) of Rh_2MnZ (Z = Sn, Pb, Tl) alloys.

| Compounds	M^{Rh}	M^{Mn}	M^Z	$M^{interstitial}$	M^{tot}	T_C
Rh_2MnSn	0.431	3.853	-0.0119	0.083	4.786	547
	0.45 [22]	3.73 [22]			4.60 [22]	435 [22]
	0.43 [23]	3.81 [23]	-0.01 [23]	0.04 [23]	4.72 [23]	410 [62]
	0.411 [24]	3.636 [24]	-0.004 [24]	0.249 [24]	4.704 [24]	420 [63]
	0.38 [30]	3.77 [30]	-0.016 [30]		4.51 [30]	431 [64]
	0.393 [32]	3.831 [32]	-0.010 [32]		4.607 [32]	
	0.310 [37]	4.075 [37]	-0.039 [37]		4.74 [37]	
Rh_2MnPb	0.424	3.882	-0.0079	0.077	4.802	463
	0.45 [22]	3.69 [22]			4.58 [22]	423 [22]
	0.401 [24]	3.673 [24]	-0.0011 [24]	0.265 [24]	4.741 [24]	338 [65]
	0.43 [30]	3.79 [30]	0.006 [30]		4.66 [30]	
	0.383 [32]	3.888 [32]	-0.009 [32]		4.644 [32]	
Rh_2MnTl	0.305	3.808	-0.022	0.026	4.424	103
	0.266 [32]	3.765 [32]	-0.027 [32]		4.27 [32]	
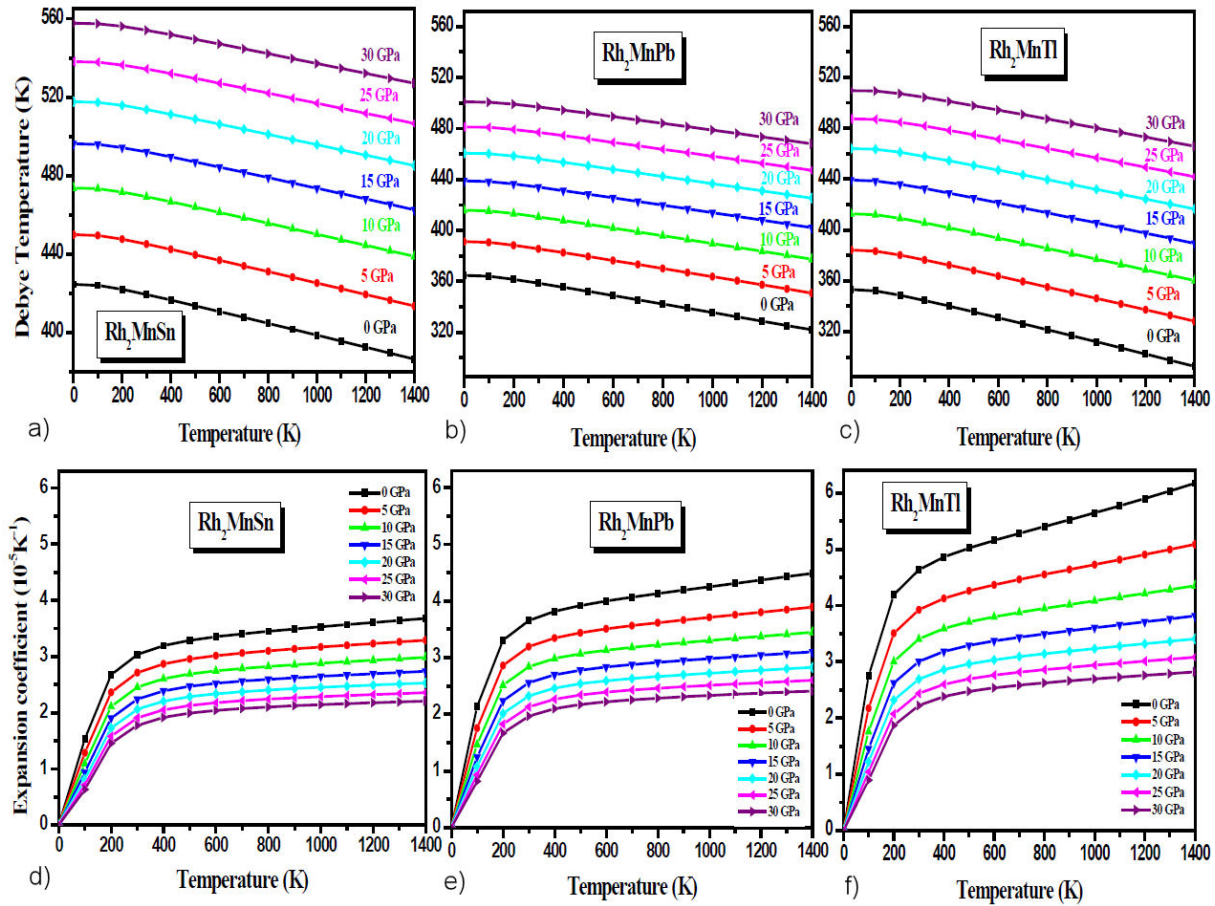
FIGURE 5. Variation of Debye temperature (θ_D) for a) Rh$_2$MnSn, b) Rh$_2$MnPb, c) Rh$_2$MnTl, and thermal expansion coefficient (α) for d) Rh$_2$MnSn, e) Rh$_2$MnPb, f) Rh$_2$MnTl as function of temperature for different pressures.

Figure 4 shows the variation of volume unit cell and bulk modulus versus pressure under various temperature values. It is clear that for all the herein compounds, the volume decreases (the bulk modulus increases) gradually with increasing pressure. Furthermore, as the temperature increases, the volume increases (the bulk modulus decreases) slowly. Due to the high rate of temperature increase, we can therefore conclude that the effect of temperature on material is dominant and leads to a reduction in hardness. At ambient temperature and 0 GPa pressure, the obtained values of volume for Rh$_2$MnSn, Rh$_2$MnPb and Rh$_2$MnTl compounds are 424.82 ($a.u.^3$), 447.25 ($a.u.^3$) and 440.22 ($a.u.^3$), respectively, and those of bulk modulus are 171.35 GPa, 152.06 GPa and 140.86 GPa, respectively.

In addition, the evolution of Debye temperature (θ_D) and thermal expansion coefficient α versus temperature at different pressures is displayed in Fig. 5. At 0 K, the Debye temperature increases from 424 K at 0 GPa to 557 at 30 GPa, from 364 K at 0 GPa to 501 at 30 GPa, from 353 K at 0 GPa to 509 at 30 GPa for Rh$_2$MnSn, Rh$_2$MnPb and Rh$_2$MnTl Heusler alloys respectively. It has a negligible variation from 0 to 100 K. In the temperature range from 100 to 1400 K, we distinguish that the thermal expansion coefficient decreases slowly with increments of temperature at a given pressure.

It is also observed from the Fig. 5 that the thermal expansion coefficient increases dramatically while temperature still 200 K. Above this value, it takes another curvature and it increases weakly with raising temperature for all the investigated compounds. It is noted that the effect of temperature becomes less. The thermal expansion coefficient decreases when an external pressure varies from 0 GPa to 30 GPa. This influence is slight for low temperatures but it becomes substantial as the temperature increases. The calculated values of α at zero pressure and room temperature are equal to 3.03×10^{-5} K^{-1}, 3.65×10^{-5} K^{-1} and 4.63×10^{-5} K^{-1} for Rh$_2$MnSn, Rh$_2$MnPb and Rh$_2$MnTl, respectively.

Additionally, the temperature effects on the specific heat (C_P) at constant pressure and specific heat (C_V) at constant volume parameters at different pressures are shown in Fig. 6.

At low temperatures, the variation of C_P and C_V is proportional to the Debye law ($\cong T^3$). However, at high temperature and for different values of pressure, in particular after 900 K, the evolution of C_V is according to the form $\cong 3R$. Thus, it tends to the classical limit of Dulong-Petit which is common to all crystalline solids [68]. The obtained C_V are about 98.8, 99.1 and 99.1 J.mol$^{-1}\cdot$K^{-1} for Rh$_2$MnSn, Rh$_2$MnPb and Rh$_2$MnTl, respectively. It is noted here that the effect of the temperature is bigger than that of the pres-
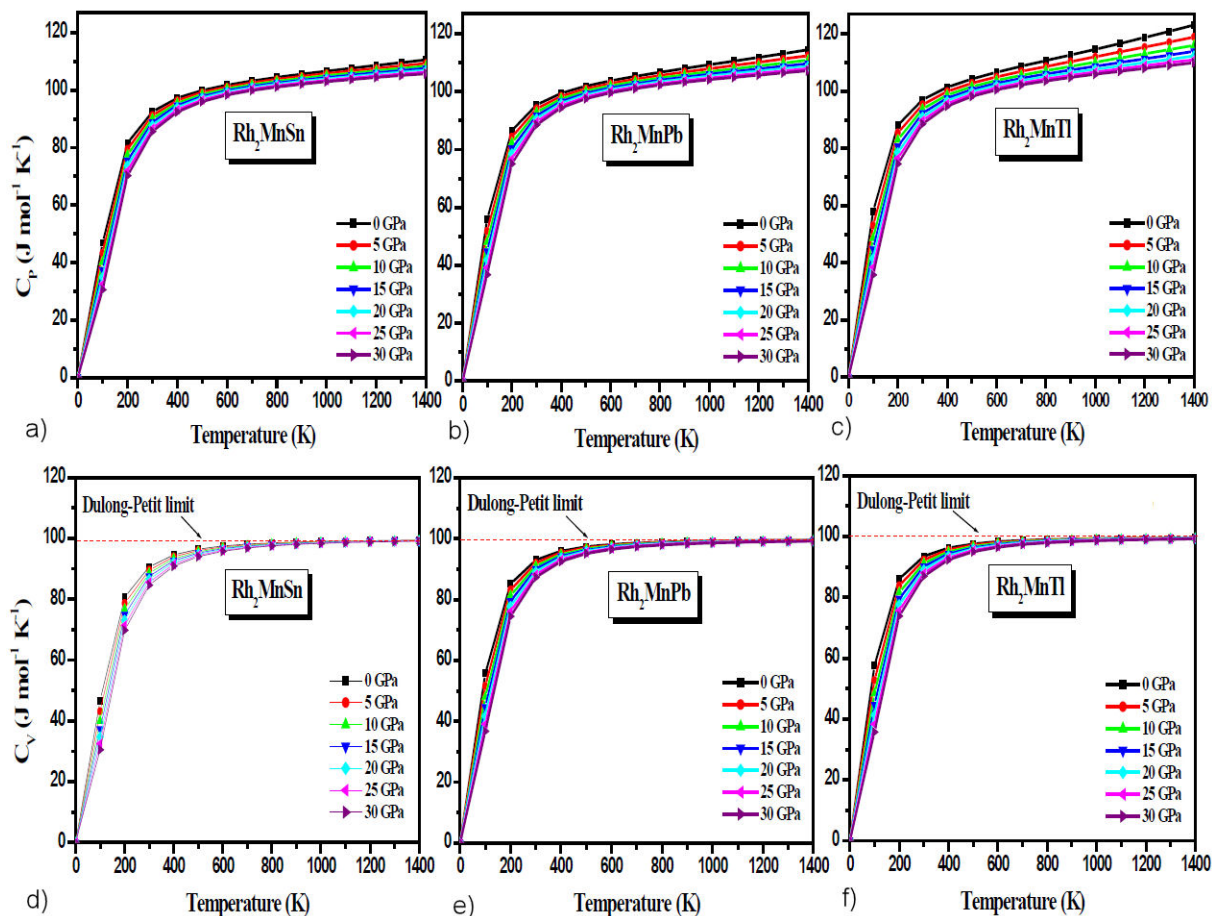
FIGURE 6. Variation of specific heat (C_P) at constant pressure for a) Rh$_2$MnSn, b) Rh$_2$MnPb, c) Rh$_2$MnTl and specific heat (C_V) at constant volume parameters for d) Rh$_2$MnSn, e) Rh$_2$MnPb, f) Rh$_2$MnTl as function of temperature for different pressures.

sure on the heat capacity. Moreover, the heat capacity (C_P) increases moderately when the temperature varies above 200 K for diverse pressures.

At zero pressure and room temperature, our obtained results for C_V are found to be 92.99, 90.66 and 93.49 J.mol^{-1}·K^{-1} and for C_P are equal to 92.45, 95.42 and 97.06 J·mol^{-1}·K^{-1} for Rh$_2$MnSn, Rh$_2$MnPb and Rh$_2$MnTl alloys, respectively.

5. Conclusion

We have investigated in detail the full-Heusler compounds Rh$_2$ MnZ (Z= Sn, Pb, Tl) using full-potential linearized augmented plane wave (FP-LAPW) method in the framework of density functional theory (DFT) within PBE-GGA for structural stabilities, elastic, electronic, magnetic and thermodynamic properties. Our calculations show that the AlCu$_2$Mn-type structure is more stable than Hg$_2$CuTi-type structure at the equilibrium volume for the systems under study. The obtained results for equilibrium lattices constant and bulk modulus are in good agreement with the previously calculated results. Also, the plots of density of states establish that Rh$_2$MnZ (Z = Sn, Pb, Tl) compounds possess ferro-

magnetic and metallic character. Furthermore, the calculated magnetic moments are in qualitative agreement with available experimental and theoretical values. The contribution to magnetic moment in these ferromagnetic compounds comes mainly from Mn atom. The magnetic properties reveal that these compounds have a ferromagnetic coupling between Rh and Mn atoms whereas anti-ferromagnetic coupling between Rh and Sn (Pb, Tl) atoms. Regarding the elastic properties, all compounds studied here satisfy the mechanical stability criteria, confirming the stability of the AlCu$_2$Mn-type structure. These alloys are found to be elastically anisotropic and have a ductile behavior. The values of elastic constants and their elastic moduli parameters are very close to those existing in the literature. We have also calculated the thermodynamic properties including volume unit cell, bulk modulus, Debye temperature, thermal expansion coefficient and specific heat capacities, at a temperature range from 0 to 1400 K and pressure from 0 to 30 GPa within the quasi-harmonic Debye approach implemented in the Gibbs2 code. Finally, we hope that our theoretical results on Rh-based Heusler alloys may provide a good baseline data to experimentalists for future spintronic application.

Acknowledgments

Conflicts of interest

The authors declare that they have no competing interests.

Authors' contributions

B. Benichou designed, coordinated this research and drafted the manuscript. H. Bouchenafa carried out a part of calculations and plotted some figures. Z. Nabi participated in research coordination and manuscript drafting. B. Bouabdallah participated in calculations and conceived of the study. The authors read and approved the final manuscript.

---

1. I. Galanakis, P. Mavropoulos, P.H. Dederichs, Electronic structure and Slater-Pauling behaviour in half-metallic Heusler alloys calculated from first principles, *J. Phys. D: Appl. Phys.* **39** (2006) 765, `https://doi:10.1088/0022-3727/39/5/S01`.

2. H.C. Kandpal, G.H. Fecher, C. Felser, Calculated electronic and magne tic properties of the half-metallic, transition metal based Heusler comp ounds, *J. Phys. D: Appl. Phys.* **40** (2007) 1507, `https://doi.org/10.1088/0022-3727/40/6/S01`.

3. B. Benichou, H. Bouchenafa, Z. Nabi and B. Bouabdallah, Ab initio investigation of the electronic structure, elastic and magnetic properties of quaternary Heusler alloy $Cu_2MnSn_{1-x}In_x$ (x = 0, 0.25, 0.5, 0.75, 1), *Rev. Mex. Fis.* **65** (2019) 468, `https://doi.org/10.31349/revmexfis.65.468`.

4. M. Ram, A. Saxena, A.E. Aly and A. Shankar, Half-metallicity in new Heusler alloys Mn_2ScZ (Z = Si, Ge, Sn), *RSC Adv.* **10** (2020) 7661, `https://doi.org/10.1039/C9RA09303F`.

5. R. Murugeswari, M. Manikandan, R. Rajeswarapalanichamy and A. Milton Franklin Benial, Structural, elastic, magnetic and electronic properties of Ti-based Heusler alloys, *Int. J. Mod. Phys. B* **34** (2020) 2050055-1, `https://doi.org/10.1142/S0217979220500551`.

6. M. Wakeel *et al.,* Structural, electronic, and magnetic properties of pal ladium based full Heusler compounds: DFT study, *Phys. B: Phys. Con dens. Matter.* **608** (2021) 412716, `https://doi.org/10.1016/j.physb.2020.412716`.

7. G.H. Fecher, Y. He, and C. Felser, Composition-dependent transition in the magnetocrystalline anisotropy of tetragonal Heusler alloys Rh_2TSb (T = Fe, Co), *Phys. Rev. Mater.* **5** (2021) 054404-1, `https://doi.org/10.1103/PhysRevMaterials.5.054404`.

8. R. Prakash and G. Kalpana, Prediction of structural, electronic and magnetic properties of full Heusler alloys Ir_2YSi (Y = Sc, Ti, V, Cr, Mn, Fe, Co, and Ni) via first-principles calculation, *AIP Adv.* **11** (2021) 015042-1, `https://doi.org/10.1063/9.0000101`.

9. O.T. Uto, P.O. Adebambo, J.O. Akinlami, S. Kenmoe, G.A. Adebayo, Electronic, structural, mechanical, and thermodynamic properties of CoYSb (Y = Cr, Mo, W) half-Heusler compounds as potential spintronic materials, *Solids* **3** (2022) 22, `https://doi.org/10.3390/solids3010002`.

10. Y. Lee, J.Y. Rhee, B.N. Harmon, Generalized susceptibility of the magnetic shape-memory alloy Ni_2MnGa, *Phys. Rev. B* **66** (2002) 054424-1, `https://doi.org/10.1103/PhysRevB.66.054424`.

11. K. Ullakko, J.K. Huang, C. Kantner, V.V. Kokorin, R.C.O. Handley, Large magnetic field induced strains in Ni_2MnGa single crystals, *Appl. Phys. Lett.* **69** (1996) 1966, `https://doi.org/10.1063/1.117637`.

12. J.M. MacLaren, Role of alloying on the shape memory effect in Ni_2Mn Ga, *J. Appl. Phys.* **91** (2002) 7801, `https://doi.org/10.1063/1.1449440`.

13. K.A. Kilian, R.H. Victora, Electronic structure of Ni_2MnIn for use in s pin injection, *J. Appl. Phys.* **87** (2000) 7064, `https://doi.org/10.1063/1.372932`.

14. A. Ayuela, J. Enkovaara, K. Ullakko, R.H. Nieminen, Structural properties of magnetic Heusler alloys, *J. Phys : Condens. Matter.* **11** (1999) 2017, `https://doi.org/10.1088/0953-8984/11/8/014`.

15. J.C. Suits, Structural instability in new magnetic Heusler compounds, *Solid. State. Commun.* **18** (1976) 423, `https://doi.org/10.1016/0038-1098(76)90040-5`.

16. R.G. Pillay, P.N. Tandon, Hyperfine magnetic field at Sn in Heusler alloys Rh_2MnSn and Rh_2NiSn, *Phys. Stat. Sol. (a)* **45** (1978) K109, `https://doi.org/10.1002/pssa.2210450248`.

17. R.G. Pillay, A.K. Grover, P.N. Tandon, L.D. Khoi, P. Veillet, NMR and Mössbauer effect studies in ferromagnetic Rh_2MnPb and Rh_2MnSb, *J. Magn. Magn. Mater.* **15/18** (1980) 647, `https://doi.org/10.1016/0304-8853(80)90703-9`.

18. S.K. Dhar, A.K. Grover, S.K. Malik, R. Vijayaraghavan, Peaks in low field a.c. susceptibility of ferromagnetic Heusler alloys, *Solid. State. Commun.* **33** (1980) 545, `https://doi.org/10.1016/0038-1098(80)90856-X`.

19. S. Jha et *al.,* Site and probe dependence of hyperfine magnetic field in $L2_1$ Heusler alloys X_2MnZ (X = Ni, Cu, Rh, Pd and Z = Ga, Ge, In, Sn, Pb), *Hyperfine Interact.* **16** (1983) 685, `https://doi.org/10.1007/BF02147342`.

20. K.H.J. Buschow, P.G. van Engen, R. Jongebreur, Magneto-optical properties of metallic ferromagnetic materials, *J. Magn. Magn. Mater.* **38** (1983) 1, `https://doi.org/10.1016/0304-8853(83)90097-5`.

21. H.P.J. Wijn, Magnetic properties of metals. Alloys and compounds of d-elements with main group elements. Part 2, ed. Landolt-Börnstein - Group III Condensed Matter (Springer Materials, Germany, 1988), pp.75-184.

22. Y. Kurtulus, R. Dronskowski, D. Samolyuk, V.P. Antropov, Electronic structure and magnetic exchange coupling in ferromagnetic full Heusler alloys, *Phys. Rev. B* **71** (2005) 014425, https://doi.org/10.1103/PhysRevB.71.014425.

23. S. Berri *et al.,* Study of structural, electronic and magnetic properties of Rh_2MnX (X = Al, Ge and Sn) Heusler alloys using GGA-WC and GGA+U approaches, *Phys. B : Condens. Matter.* **418** (2013) 58, https://doi.org/10.1016/j.physb.2013.03.002.

24. F.Z. Benkhelifa, A. Lekhal, S. Méçabih, GGA and GGA+U Description of Structural, magnetic, and elastic properties of Rh_2MnZ (Z = Ge, Sn, and Pb), *J. Supercond. Nov. Magn.* **26** (2013) 2573, https://doi.org/10.1007/s10948-012-1815-7.

25. F.Z. Benkhelifa, A. Lekhal, S. Méçabih, B. Abbar, B. Bouhafs, Electronic structure, magnetic and thermal properties of Rh_2MnZ (Z = Ge, Sn, Pb) compounds under pressure from ab-initio quasi-harmonic method, *J. Magn. Magn. Mater.* **371** (2014) 130, https://dx.doi.org/10.1016/j.jmmm.2014.07.048.

26. M. Yin, P. Nash, Standard enthalpies of formation of selected Rh_2YZ Heusler compounds, *J. Alloy. Compd.* **650** (2015) 925, https://doi.org/10.1016/j.jallcom.2015.08.054.

27. M. Mebrek *et al.,* Theoretical investigation of electronic structures, elastic, and magnetic properties of Rh_2CrGe full-Heusler alloy, *Acta. Phys. Pol. (a)* **136** (2019) 454, https://doi.org/10.12693/APhysPolA.136.454.

28. L. Boumia *et al.,* Structural, electronic and magnetic properties of new full Heusler alloys Rh_2CrZ (Z = Al, Ga, In): First-principles calculatio ns, *Chin. J. Phys.* **59** (2019) 281, https://doi.org/10.1016/j.cjph.2019.04.002.

29. J.C. Suits, New magnetic compounds with Heusler and Heusler-related structures, *Phys. Rev. B* **14** (1976) 4131, https://doi.org/10.1103/PhysRevB.14.4131.

30. M. Pugacheva, A. Jezierski, Dependence of the magnetic moment on the local atomic order in Rh_2MnX Heusler alloys, *J. Magn. Magn. Mater.* **151** (1995) 202, https://doi.org/10.1016/0304-8853(95)00372-X.

31. A. Jezierski, M. Pugaczowa-Michalska, J.A. Morkowski, A. Szajek, Elec tronic structure and magnetic Properties of intermetallic alloys, *Acta. P hys. Pol. (a)* **91** (1997) 151, https://dx.doi.org/10.12693/APhysPolA.91.151.

32. I. Galanakis, P.H. Dederichs, Slater-Pauling behavior and origin of the half-metallicity of the full-Heusler alloys, *Phys. Rev. B* **66** (2002) 174429, https://doi.org/10.1103/PhysRevB.66.174429.

33. P. Klaer *et al.,* Localized magnetic moments in the Heusler alloy Rh_2 MnGe, *J. Phys. D: Appl. Phys.* **42** (2009) 084001, https://doi.org/10.1088/0022-3727/42/8/084001.

34. S. Sanvito *et al.,* Accelerated discovery of new magnets in the Heusler alloy family, *Sci. Adv.* **3** (2017) e1602241, https://doi.org/10.1126/sciadv.1602241.

35. S.V. Faleev *et al.,* Origin of the tetragonal ground state of Heusler com pounds, *Phys. Rev. Appl.* **7** (2017) 034022, https://doi.org/10.1103/PhysRevApplied.7.034022.

36. F. Benzoudji *et al.,* The preference of the ferromagnetic ordering for the novel Heusler Rh_2MnTi compound, *J. Supercond. Nov. Magn.* **32** (2018) 1, https://dx.doi.org/10.1007/s10948-018-4837-y.

37. F. Aguilera-Granja, R.H.L. Aguilera-del-Toro, J. Morán-López, A first principles systematic study of the structural, electronic, and magnetic properties of Heusler X_2MnZ with X = Fe, Co, Ni, Cu, Ru, Rh, Pd, Ag, Pt, Au and Z = Al, Si, Ga, Ge, In and Sn, *Mater. Res. Express.* **6** (2019) 106118, https://dx.doi.org/10.1088/2053-1591/ab243c.

38. A. Mentefa *et al.,* First-principles calculations to investigate structural, electronic, elastic, magnetic, and thermodynamic properties of full-Heusler Rh_2MnZ (Z = Zr, Hf), *J. Supercond. Nov. Magn.* **34** (2021) 269, https://doi.org/10.1007/s10948-020-05741-6.

39. E. Güler, M. Güler, S. Ugur, and G. Ugur, First principles study of electronic, elastic, optical and magnetic properties of Rh_2MnX (X = Ti, Hf, Sc, Zr, Zn) Heusler alloys, *Int. J. Quantum. Chem.* **121** (2021) e26606, https://doi.org/10.1002/qua.26606.

40. J.C. Slater, Energy Band Calculations by the Augmented Plane Wave Method, *Adv. Quant. Chem.* **1** (1964) 35, https://doi.org/10.1016/S0065-3276(08)60374-3.

41. P. Blaha *et al.*, WIEN2k: an augmented plane wave plus local orbitals program for calculating crystal properties, (University of Technology, Vienna, Austria, 2019), pp. 1-287.

42. P. Hohenberg, W. Kohn, Inhomogeneous Electron Gas, *Phys. Rev. B.* **136** (1964) B864, https://doi.org/10.1103/PhysRev.136.B864.

43. W. Kohn, L.J. Sham, Self-Consistent Equations Including Exchange a nd Correlation Effects, *Phys. Rev.* **140** (1965) A1133, https://doi.org/10.1103/PhysRev.140.A1133.

44. J.P. Perdew, K. Burke, M. Ernzerhof, Generalized Gradient Approxim ation Made Simple, *Phys. Rev. Lett.* **77** (1996) 3865, https://doi.org/10.1103/PhysRevLett.77.3865.

45. A. Kokalj, Computer graphics and graphical user interfaces as tools in simulations of matter at the atomic scale, *Comp. Mater. Sci.* **28** (2003) 155, https://doi.org/10.1016/S0927-0256(03)00104-6.

46. F.D. Murnaghan, The compressibility of media under extreme pressures, *Proc Natl. Acad. Sci. USA* **30** (1944) 244, https://doi.org/10.1073/pnas.30.9.244.

47. M. Born, K. Huang, Dynamical theory of crystal lattices (Clarendon Press, Oxford, 1954), pp. 837-838.

48. J. Wang, S. Vip, S.R. Phillpot, D. Wolf, Crystal instabilities at finite st rain, *Phys. Rev. Lett.* **71** (1993) 4182, https://doi.org/10.1103/PhysRevLett.71.4182.

49. W. Voigt, Lehrbuch der kristallphysik (mit ausschluss der kristalloptik), (ed.) B G Teubner Verlag (Nachdruck der ersten Aufl, Germany, 1928), pp.1-978.

50. A. Reuss, Z. Angew, Berechnung der fließgrenze von mischkristallen auf grund der plastizitätsbedingung für einkristalle., *Appl. Math. Mech.* **9** (1929) 49, `https://doi.org/10.1002/zamm.19290090104`.

51. R. Hill, The elastic behaviour of a crystalline aggregate, *Proc. Phys. Soc. A* **65** (1952) 349, `https://doi.org/10.1088/0370-1298/65/5/307`.

52. D.G. Pettifor, Theoretical predictions of structure and related properti es of intermetallics, *Mater. Sci. Technol.* **8** (1992) 345, `https://doi.org/10.1179/mst.1992.8.4.345`.

53. S.F. Pugh, XCII. Relations between the elastic moduli and the plastic properties of polycrystalline pure metals, *Philos. Mag.* **45** (1954) 823, `https://doi.org/10.1080/14786440808520496`.

54. J. Haines, J.M. Léger, G. Bocquillon, Synthesis and design of superhard materials, *Annu. Rev. Mater. Res.* **31** (2001) 1, `https://doi.org/10.1146/annurev.matsci.31.1.1`.

55. F. Chu, Y. He, D.J. Thoma, T.E. Mitchell, Elastic constants of the C15 laves phase compound NbCr$_2$, *Scripta. Metali. Mater.* **33** (1995) 1295, `https://doi.org/10.1016/0956-716X(95)00357-2`.

56. P. Wachter, M. Filzmoser, J. Rebizant, Electronic and elastic properties of the light actinide tellurides, *Phys. B: Condens. Matter.* **293** (2001) 199, `https://dx.doi.org/10.1016/S0921-4526(00)00575-5`.

57. O.L. Anderson, A simplified method for calculating the debye temperature from elastic constants, *J. Phys. Chem. Solids.* **24** (1963) 909, `https://doi.org/10.1016/0022-3697(63)90067-2`.

58. E. Schreiber, O.L. Anderson, N. Soga, Elastic constants, and their measurements (McGraw-Hill Book Co., New York, 1973), pp. 82-125.

59. M.E. Fine, L.D. Brown, H.L. Marcus, Elastic constants versus melting temperature in metals, *Scripta Metallurgica.* **18** (1984) 951, `https://doi.org/10.1016/0036-9748(84)90267-9`.

60. S.E. Kulkova, S.V. Eremeev, T. Kakeshita, S.S. Kulkov, G.E. Rudenski, The electronic structure and magnetic properties of full- and half-Heus ler alloys, *Mater. Trans.* **47** (2006) 599, `https://doi.org/10.2320/matertrans.47.599`.

61. N. Kervan, S. Kervan, O. Canko, M. Atis, F. Taskin, Half-metallic ferri magnetism in the Mn$_2$NbAl full-Heusler compound: a first-principles st udy, *J. Supercond. Nov. Magn.* **29** (2016) 187, `https://doi.org/10.1007/s10948-015-3228-x`.

62. J.C. Suits, New magnetic compounds with Heusler and Heusler-related structures, *AIP Conference Proceedings.* **29** (1976) 587, `https://dx.doi.org/10.1063/1.30466`.

63. R.G. Pillay, P.N. Tandon, H.G. Devare, N.K. Jaggi, K.R.P.M. Rao, Hyperfine interaction studies in ferromagnetic Rh$_2$MnSn, *Solid State Commun.* **23** (1977) 439, `https://dx.doi.org/10.1016/0038-1098(77)91003-1`.

64. Y. Adachi *et al.,* Pressure effect on the Curie temperature of the Heusler alloys Rh$_2$MnZ (Z = Sn, Ge), *J. Alloys Compd.* **383** (2004) 37, `https://dx.doi.org/10.1016/j.jallcom.2004.04.003`.

65. S. Jha, R.D. Black, G.M. Julian, J.W. Blue, D.C. Liu, Hyperfine magnetic field at Cd impurity site in L2$_1$ Heusler alloys Rh$_2$MnGe and Rh$_2$MnPb by TDPAC technique, *J. Appl. Phys.* **50** (1979) 7507, `https://dx.doi.org/10.1063/1.326881`.

66. M.A. Blanco, E. Francisco, V. Luaña, GIBBS: isothermal-isobaric ther modynamics of solids from energy curves using a quasi-harmonic Debye model, *Computer. Phys. Commun.* **158** (2004) 57, `https://doi.org/10.1016/j.comphy.2003.12.001`.

67. S.A. Khandy, I. Islam, Z.S. Ganai, D.C. Gupta, K.A. Parrey, High-tem perature and high-pressure study of electronic and thermal properties of PbTaO$_3$ and SnAlO$_3$ metal perovskites by density functional theory calculations, *J. Electron. Mater.* **47** (2018) 436, `https://doi.org/10.1007/s11664-017-5785-1`.

68. A.-T. Petit and P-L. Dulong, Recherche sur quelques points importants de la Théorie de la Chaleur, *Ann. Chim. Phys.* **10** (1819) 395; [English translation in *Ann. Philos.* **14** (1819) 189].